Chapter 5

Nanotubes Should Enhance Body Armor

Nanotubes should enhance body-armor stealth and strength. This proposed research direction extrapolates applied and theoretical findings. We present a review of nanoenhanced materials, our experimental analysis of body-armor performance, and a proposed adaptive camouflage that support the informed extrapolation.

Researchers have demonstrated that nanotube additives strengthen fibers [264] [6] and toughen ceramics [371], [428], [482], [481], [489] and so can help body armor resist ballistic impacts. Researchers have also demonstrated that nanoparticle-treated fabric armor can adapt to stimuli [272] and can reduce physiological costs of wearing armor.

Nanotubes can reduce physiological costs such as bruising because strengthened materials can reduce body-armor deformation. Nanoparticle-enhanced armor stiffens on impact to reduce deformation [272] and so should reduce or eliminate the bruising effect of bullets that deform soft body armor. The enhanced materials may further reduce heat exhaustion because they can decrease body-armor stiffness, thickness, and weight as well as increase body-armor heat-carrying capacity.

We modeled body-armor bruising effects to study a physiological cost of wearing armor. Field experiments measured body-armor performance with a bruise profile. We modeled the bruising effect of nonpenetrating bullet impacts with statistical and fuzzy

methods and a baseball comparison. The analysis techniques can also model the bruising effects of nano-enhanced body armor.

Nanotube electronics should adapt camouflage patterns to disguise armor. A proposed adaptive camouflage uses nanotubes and nanoparticles to help conceal armor. The proposed camouflage uses octopus-model artificial color organs to display changing camouflage patterns and uses nanotube sensors and processors to coordinate the displayed patterns.

Section 5.1 discusses how nanomaterials can enhance body armor performance. Section 5.2 summarizes our study of soft body-armor performance in terms of a bruise profile. The Appendix presents the experimental results in detail. Section 5.3 proposes an octopus-model adaptive camouflage that uses nanotubes and nanoparticles to help disguise body armor.

5.1 Nanomaterials Can Enhance Body-Armor Strength and Adaptability

Nanotubes and nanoparticles can strengthen armor materials and make adaptive and programmable armor materials. Nanotubes can strengthen polymer fibers and ceramic composites in body armor whereas nanoparticles can help make armor fabric more flexible until external stimuli causes the armor to stiffen.

Body armor materials include textiles, fiber composites, ceramic composites, and metal. Military flak jackets are a compromise between mobility and protection and can consist of camouflaged flexible Kevlar fabrics that cover the torso and composite or metal-plate inserts that reinforce key areas. Mobility is important because it makes the armor user harder to target.

The flexible fabrics allow more mobility but do not stop rifle bullets [454]. The metal or composite plates stop rifle bullets but are heavy so protect only parts of the torso. The flak jackets optimize ballistic protection by covering the torso and shoulders with flexible fabric and reinforcing the front and back with ceramic or metal plates.

Flak jackets optimize mobility by exposing the limbs and joints. The joints are unprotected to retain mobility because thick fabric armor can be stiff and resists bending. An effective camouflage should enhance armor stealth and further improve armor performance.

Alumina ceramic-composite armor can be harder than bullets and can often fracture a bullet on impact without deforming. But ceramics are inflexible and heavy and inhibit movement and heat dissipation. Thin and flexible armor give the armor user more mobility and reduce physiological costs such as heat exhaustion [180]. Nanotube additives strengthen ceramics [371], [428], [482], [481], [489] and polymers [6]. The strengthened materials can make armor thinner and lighter and so reduce physiological costs.

Researchers have found that adding 0.1 wt % carbon nanotubes to alumina composite increases the fracture toughness from 3.7 to 4.9 MPa·m$^{1/2}$ [428] and that adding 10 wt % nanotubes nearly triples the fracture toughness of nanocrystalline alumina (9.7 MPa·m$^{1/2}$) [489]. Nanotube-enhanced alumina ceramics permit armor designs that use thinner and lighter ceramic plates to cover a larger area and so can add mobility and reduce physiological costs. Nanotubes might also toughen boron carbide that has a diamond-like hardness of about 30 GPa but that fails to resist high-velocity bullets [79].

The textile and fiber-composite soft body armor resist bullet penetration because the fibers distribute a bullet's crushing force over a large area when the bullet deforms the armor [302]. The two most common ballistic fabrics in the United States are Kevlar and Spectra Shield [454]. Kevlar is an aramid or poly-(p-phenylene terephthalamide)

(PPTA) fiber and its fabrics are woven [301]. Zylon or poly(p-phenylene benzobisoxazole) (PBO) fibers are stronger than Kevlar but Kevlar is the most popular armor fiber.

Spectra Shield consists of ultra high molecular weight polyethylene and its fibers are resin-bonded instead of woven and lie parallel in each criss-crossing sheet [454]. A ballistic fabric resists bullets better if its threads consist of numerous fine microfibers [301].

Nanotube additives strengthen polymers to make stronger fibers and fabrics. Ballistic fabrics absorb and disperse an impact's energy from the struck fibers to other fibers in the fabric [454]. This dissipation reduces the severity of the impact when the armor stops the bullet.

Nanotube-strengthened fibers can absorb more energy. Researchers have strengthened Zylon or PBO fibers with multiwall nanotubes: Adding 10 wt% MWNT increases PBO fiber's tensile strength by 50% [264].

Nanoparticle-treated fabrics recruit more fibers to disperse a bullet's impact energy. The silica nanoparticle-based shear thickening fluid (STF) hardens on impact and reduces sliding between fibers. This helps a struck fiber disperse the impact energy to neighboring fibers.

Researchers have shown that a STF-treated Kevlar armor resists ice pick thrusts that penetrate untreated armor [143] and have shown that the STF-treated armor deforms less on bullet impact than untreated armor [272] [232] (see Figure 5.1). STF-treated armor can be thinner and so can be more flexible. This should help armor designs that protect limbs and joints.

Magnetic rheologic (MR) fluids harden in magnetic fields so a MR-treated armor can have programmable toughness. The iron nanoparticles turn a MR fluid into a solid when magnetic fields cause the nanoparticles to agglomerate [1] [2].

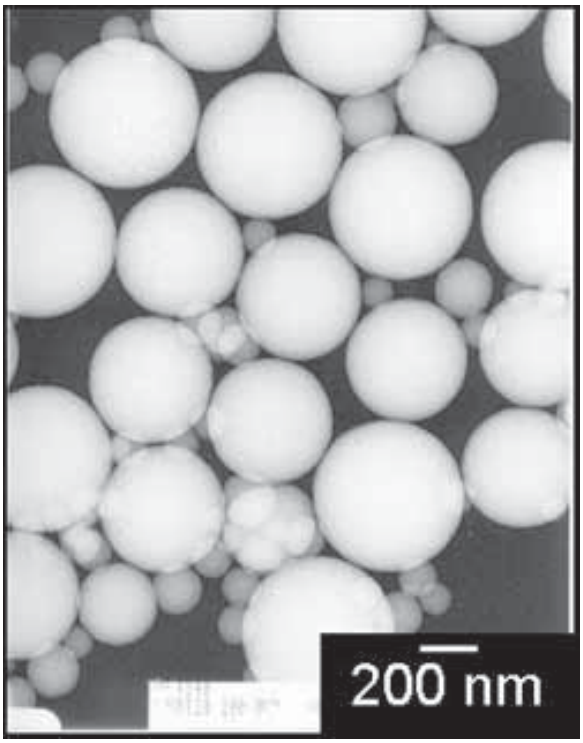

(a) Silica Nanoparticle

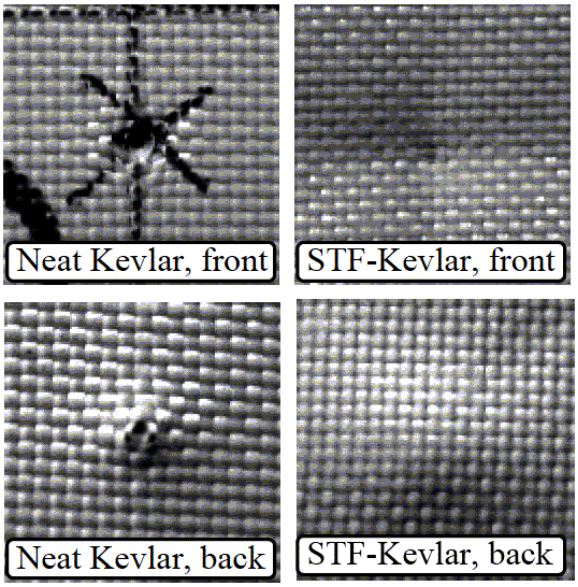

(b) Resist Spike Impact

(c) Plain Kevlar

(d) STR-treated Kevlar

Figure 5.1: Shear thickening fluid enhances Kevlar armor (a) Scanning electron micrograph of silica nanoparticles in a shear thickening fluid. (b) STF-treated Kevlar resists spike penetration. (c) Untreated Kevlar shows larger deformation than (d) STF-treated Kevlar. With permission from Wetzel et al. 2004 [143].

Deshmukh et al. have found that a MR-treated cellular solid can modulate total energy absorption by a factor of 50-fold for small volume fractions of the fluid ($\approx$15%) using magnetic fields varying from 0 to 0.2 Tesla [116]. MR fluid-impregnated armor fabric should recruit fibers to disperse impact energy similar to the STF-treated armor because the fabrics have interfiber spacing that resembles the experimental substance in [116]. These enhanced fabric armor might prevent a bullet impact from bruising the tissue beneath the armor.

5.2 A Bruise Profile Measures Soft Body Armor Performance

A bruise profile can measure the performance of nanoparticle-enhanced body armor. Field experiments used a bruise profile to model the blunt injury effects of a handgun bullet that deformed generic Kevlar fabric armor against a backing material that simulated tissue. The bruise profile measured armor performance in terms of a physiological cost. This section summarizes our experimental findings based on Kevlar-fabric armor. The Appendix contains the complete report.

Our analysis techniques can also model bruising effects in nanoenhanced armor. The analysis techniques can evaluate the performance of the enhanced armor that can reduce or eliminate bruising effects for nonpenetrating bullets.

We analyzed the experimental data statistically and found that impact deformation correlated with bullet weight and momentum better than it correlated with bullet kinetic energy. We applied a fuzzy system to predict the bruising effect of handgun bullets on body armor. This type of fuzzy analysis can learn to predict the bruising effect for nanoparticle-enhanced body armor.

We also compared handgun bullets and baseballs by shooting bullets at armor-clad Plumber's Putty targets and by pitching baseballs at bare Putty targets. The Plumber's Putty does not simulate tissue but records the impact deformation in a consistent medium.

Baseball impact depths were comparable to bullet-armor impact depths: Getting shot with a .22 caliber bullet when wearing soft body armor resembles getting hit in the bare chest with a 40-mph baseball. Getting shot with a .45 caliber bullet resembles getting hit with a 90-mph baseball.

What is the bruising effect of a bullet on soft body armor that deforms and permits the impact to affect tissue beneath the armor? Figure 5.2 shows the bruise beneath the armor after a .44 caliber bullet struck a police officer's upper left chest. The Kevlar-fabric armor stopped the bullet but the impact still injured soft tissue. Few researchers examine the bruising effect of soft body armor [226]. A national standard for armor testing [343] includes an evaluation of the so-called "backface signatures" that are the deformation in the armor's backing material after a gunshot. The standard uses modeling clay to back and record the armor deformation instead of gelatin blocks that can simulate tissue. So the backface deformation data correlate little with a bullet's bruising effect.

We examined the bruising effect with a fuzzy function approximator and a baseball analogy. Bullet impact experiments produced the bullet-armor bruise data that generated a quantitative bruise profile and a baseball-impact comparison. The bruise profile gave the depth and width of the deformation that a handgun bullet made on gelatin-backed armor (see Figure 5.3) for gelatin blocks that we made with Type 250A Ordnance Gelatin (from Kind & Knox Gelatin).

Experiments shot different caliber handgun bullets at gelatin-backed armor to produce armor deformations. The depths and widths of the deformations correlated with handgun-bullet weight, momentum, and kinetic energy. Deformation correlated the least

Figure 5.2: (a) Actual bruise from a police officer shot by a .44 caliber weapon in the line of duty while wearing soft body armor. (b) Close-up of the "backface signature" bruise in (a). Note that the bruise includes the discoloration around the wound. Photo reproduced with permission from the IACP/Du Pont Kevlar Survivors' Club.

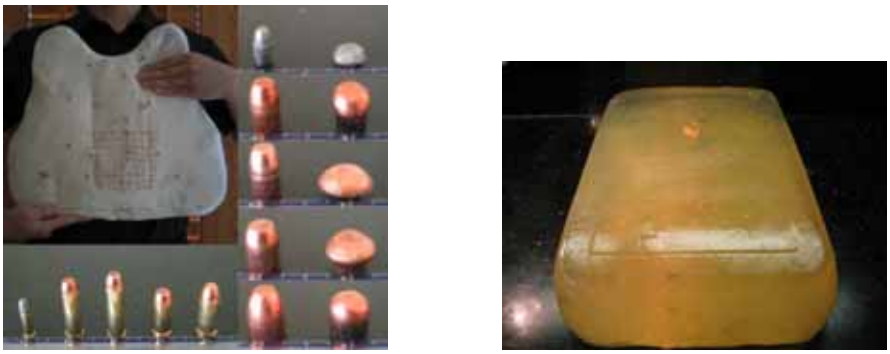

(a) Fabric Armor (b) Gelatin Block

Figure 5.3: Armor experiments used soft body armor and ordnance gelatin blocks. (a) A 14-ply Kevlar soft body armor panel (from a Superfeatherlite vest from Second Chance) and some sample cartridges (.22, .38, .357 magnum, .40, and .45 caliber). The right side of the image shows the pristine and armor-deformed bullets for the five calibers. (b) A sample 10% ordnance gelatin block. A target consisted of a generic armor-clad gelatin block. The gel block simulated tissue.

with bullet kinetic energy and did not correlate with bullet speed for experiments that varied both bullet weight and speed.

We applied a simple linear regression model

$$y \quad = \quad \beta_0 + \beta_1 x \tag{5.1}$$

to test whether bullet deformation y correlated with each of a bullet's properties: weight, momentum, kinetic energy, speed and distance to target. The null hypothesis $\mathbf{H}_0 : \beta_1 = 0$ stated that the slope β_1 of the regression line in (5.1) was zero and thus the impact deformation's depth and width (dependent variables) did not vary with a bullet's weight, momentum, kinetic energy, speed, or distance to target (independent variables). The p-value measures the credibility of $\mathbf{H}_0$. A statistical test rejects the null hypothesis $\mathbf{H}_0$ at a significance level α if the p-value is less than that significance level: Reject $\mathbf{H}_0$ if p-value $< \alpha$. A test would reject the null hypothesis $\mathbf{H}_0$ at the standard significance levels $\alpha = 0.05$ and $\alpha = 0.01$ if p-value < 0.001. Correlation coefficient R^2 measures the strength of the correlation.

Linear regression gave correlation coefficients R^2 between armor-deformation depth and bullet weight ($R^2 = 0.880$ and $p < 0.001$), momentum ($R^2 = 0.741$ and $p < 0.001$), kinetic energy ($R^2 = 0.474$ and $p < 0.001$), speed ($R^2 = 0.089$ and $p < 0.025$), and distance to target ($R^2 = 0.415$ and $p < 0.001$). This showed that the correlations for weight and momentum were statistically more significant than kinetic energy and that speed did not correlate with deformation depth.

We applied a multiple regression

$$y \quad = \quad \beta_0 + \beta_1 x_1 + \beta_2 x_2 \tag{5.2}$$

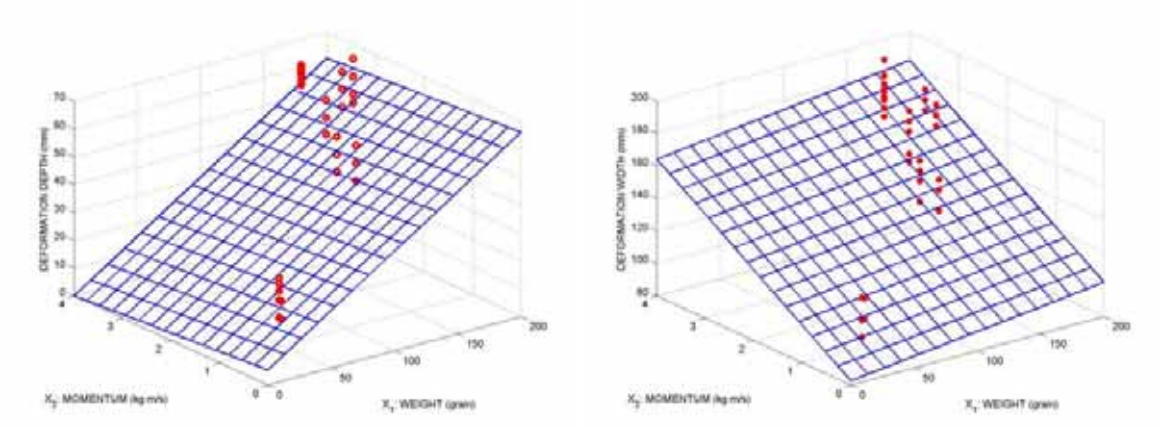

(a) DEPTH (b) WIDTH

Figure 5.4: The deformation data from gelatin-backed bullet-armor experiments that used generic Kevlar fabric armor. The figures show the complete set of experimental depth data in (a) and the width data in (b) and their fit to regression planes as functions of weight (X_1) and momentum (X_2). The regression planes consist of those points that satisfy the regression equations: $y_1 = 5.550 + 0.304x_1 - 1.361x_2$ for depth in (a) and $y_2 = 84.846 + 0.425x_1 - 0.240x_2$ for width in (b).

for combinations of a bullet's property such as weight and momentum and tested the null hypothesis $\mathbf{H}_0 : \beta_i = 0$ for $i = 0, 1, 2$ that all the parameters were statistically insignificant. This tested whether the deformation's depth and width varied with the combination of a bullet's weight and momentum. The multiple regression produced regression coefficients between deformation depth and the combination of weight and momentum ($\beta_1 = 0.304$, $p < 0.001$, $\beta_2 = -1.361$, and $p = 0.510$) and the combination of weight and kinetic energy($\beta_1 = 0.293$, $p < 0.001$, $\beta_2 = -0.006$, and $p = 0.427$). This showed that the coefficient for bullet weight was statistically more significant than for either momentum or kinetic energy. These regression tests helped guide our choice of weight and momentum as the inputs of a fuzzy system.

A fuzzy system learned from the bullet-armor experimental data to predict the bruise profile for range ammunition, generic fabric armor, and ordnance gelatin blocks. Figure 5.4 shows a set of data that tuned a fuzzy system. Impact experiments that test new

Figure 5.5: A regulation baseball and a crater of its impact. Pitching machines threw baseballs at tubs of Plumber's Putty. A chronograph measured the speed of each baseball. The baseball speeds were approximately 40, 50, 60, 70, 80, and 90 miles per hour.

armor designs would produce impact data that can tune the fuzzy system and update the bruise profiles for the new armor designs including nano-based enhancements.

Baseball experiments compared bullet-armor impacts to baseball impacts in two ways: Deformation depths in putty and the slopes of the fitted regression lines. The first way compared how the two types of projectile deformations differed. The experiments found that baseball impacts and bullet-armor impacts had similar depths in Oatey's Plumber's Putty (see Figure 5.5). The similarity of impact depths suggested that handgun shots on soft body armor would feel like baseball impacts without armor. Fast-baseball impact depths were comparable to bullet-armor impact depths: Getting shot with a .22 caliber bullet when wearing soft body armor resembles getting hit on the chest with a 40-mph baseball. Getting shot with a .45 caliber bullet resembles getting hit with a 90-mph baseball.

The second way compared the correlation and regression slopes of the two types of impacts. The experiments found that the mean depth of a baseball's impact and the depth of a bullet's armor-impact both correlated with projectile momentum (see Fig. 5.6). The baseball impacts had correlation $R^2 = 0.93$, regression equation $y = -6.155 + 5.188x$, and p-value < 0.001 where x was a baseball's momentum in kilograms meter per second

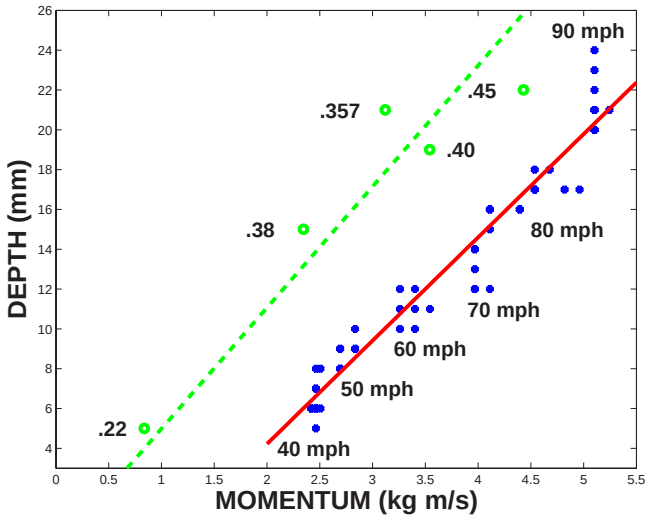

Figure 5.6: Baseball and bullet impact depths in Plumber's Putty versus momentum. The baseball impact depth correlated with baseball momentum $R^2 = 0.93$ and p-value < 0.001 for the null hypothesis: $\beta_1 = 0$. The solid line on the right is the regression line for the baseball impacts (blue dots) $y = -6.155 + 5.188x$ where x is baseball momentum and y is putty deformation depth. Only two data points fell outside of the 95% confidence bounds. Bullet-armor impact depths correlated with bullet momentum $R^2 = 0.97$. The green dashed line on the left is the regression line for the bullet-armor impacts (green circles) $y = 2.124 + 4.766x$ where x is bullet momentum and y is depth. The two regression lines have the similar slope $\beta_1 \approx 5$. A multiple regression analysis with dummy variables (Gujarati-Chow test) could not reject the null hypothesis $H_0 : \beta_1$(baseball) $= \beta_1$(armor) for the test statistics $t = 0.855$ and p-value $= 0.396$. So the test retained the null hypothesis that the two types of impacts had the same slope.

(kg m/s) and y was the putty deformation depth in millimeters (mm). The bullet-armor impacts had similar correlation $R^2 = 0.97$, regression equation $y = -2.12 + 4.76x$, and p-value < 0.001.

The putty-impact regression lines had similar slopes $\beta_1 \approx 5$ for the baseball impacts ($\beta_1 = 5.188$) and the bullet-armor impacts ($\beta_1 = 4.766$). Fig. 5.6 suggests that the two lines are parallel: Same slope with different intercepts. A modified Chow test (Gujarati-Chow test [189]) confirmed that the two putty-impact regression lines had statistically indistinguishable slopes for the slope-term test statistic $t = 0.855$ and p-value $= 0.396$.

The p-value implies that the identical-slope hypothesis must be retained at the standard significance levels $\alpha = 0.05$ and $\alpha = 0.01$.

5.3 A Proposed Octopus-Model Architecture Uses Nanotubes and Nanoparticles to Adapt Camouflage

Nanotubes can coordinate octopus-model artificial color organs to disguise body armor. The proposed adaptive camouflage models an octopus that changes skin patterns to avoid detection.

The adaptive camouflage can match a background by using nanotube signal processing to change displayed patterns. Nanotube optical sensors [484] can sample a background image. Nanotube processors can quickly [67] select a preset pattern or compose a custom pattern that optimally matches a background.

Nanotubes can interconnect the sensors, processors, and color organ by applying embedded wired connection in a flexible substrate [54] or by applying wireless connection in a distributed network (such as in [432]).

This section reviews how *Octopus vulgaris* and other cephalopods camouflage or disguise their bodies and proposes an octopus-model adaptive camouflage that uses nanotubes and nanoparticles.

5.3.1 Octopus Physiology for Camouflage

An octopus can abruptly change its appearance or mimic other animals by changing its color, texture, posture, and locomotion [325]. The octopus responds to visual input and selects an appropriate body pattern from a small set of patterns that are "hardwired" into the central nervous system [325]. The preset patterns either help the animal match its background or break up the outline of its body.

Researchers have further documented nine octopus specimens that mimic poisonous animals [352] (see Figure 5.7). These octopuses use posture and locomotion to mimic swimming fish and sea snake both in appearance and in motion.

The octopus camouflage changes whole body patterns to either blend in with the background by matching the color, brightness, and texture (see Figure 5.8(a)) or break up the body outline by displaying disruptive patterns (Figure 5.8(b)). A whole body pattern consists of organized collections of skin patches or units (see Figures 5.8(c) and 5.8(d)).

Individual skin patches have chromatophores and iridophores that display different colors, leucophores that adjust brightness, and papillae musculature that changes skin texture [325]. The chromatophores and the iridophores occur across the whole skin patch. The leucophores occur only in the central region of the patch and beneath the chromatophores and the iridophores. A skin papilla occurs exactly at the center of a patch. It contracts to stretch the patch into a spike.

The octopus camouflage is an orchestration between chromatophores, iridophores, leucophores and skin muscles [325]. *Octopus vulgaris* has up to 230 chromatophores per square millimeter of skin and devotes millions of neurons to control them [325]. Chromatophore motoneurons send pulses to expand specific sets of chromatophores in the skin. Banks of chromatophore motoneurons act in concert to produce the bars, bands, and lines in *Octopus vulgaris*' skin [325]. An octopus selects a stipple, mottle, or disruptive pattern if it sees discontinuities.

The octopuses match the background brightness by manipulating the chromatophores and the leucophores. Relaxing the dark-colored chromatophores reduces their size and uncovers the underlying leucophores that reflect the surrounding light and help match both the color and brightness of a low-light background (see Figure 5.9).

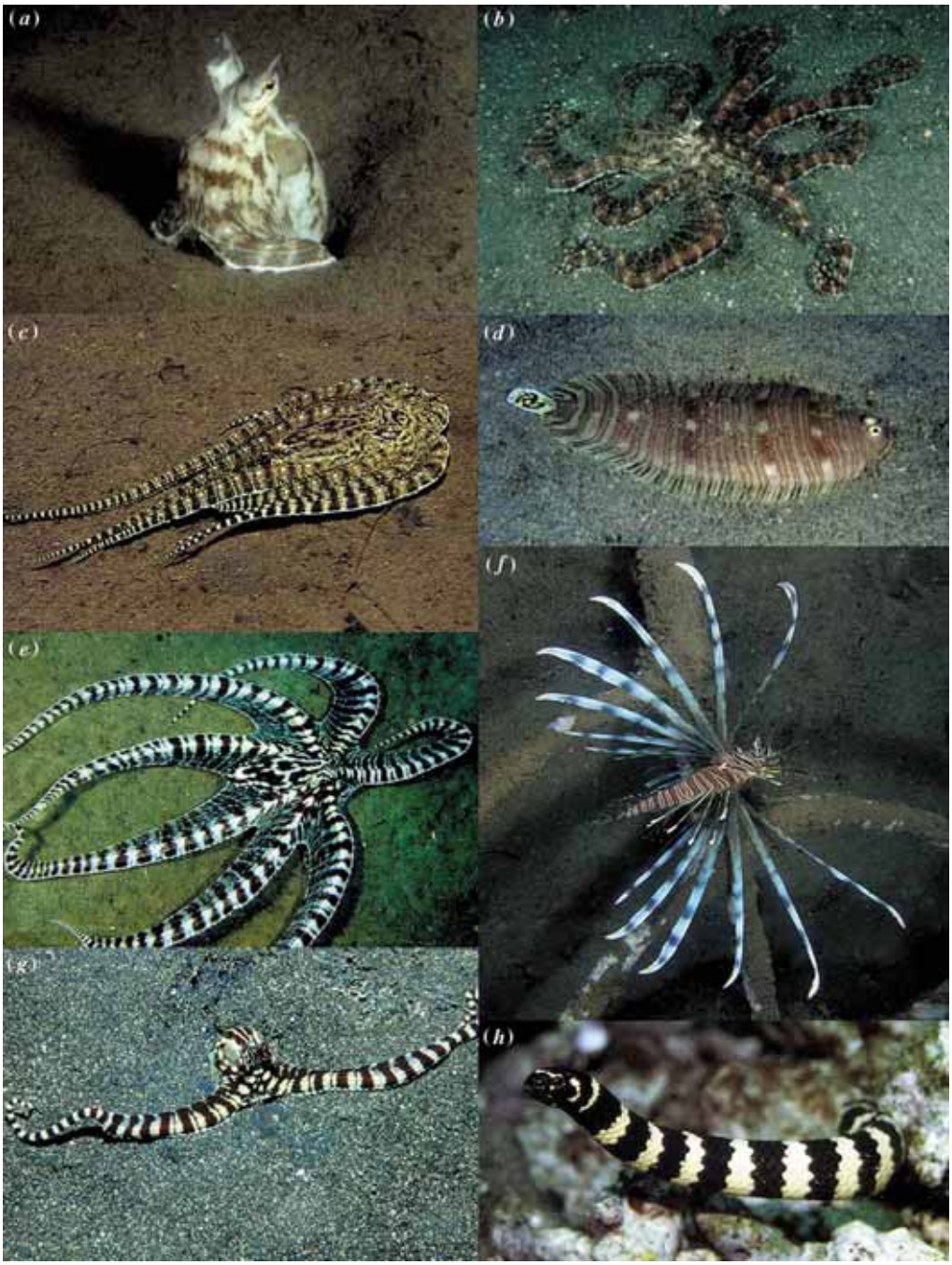

Figure 5.7: Mimic octopus (a) sentinel state in mouth of burrow; (b) normal foraging color pattern; (c) flatfish mimicry; (d) flatfish model, banded sole (Zebrias sp.); (e) lion-fish mimicry; (f) lion-fish model (Pterois sp.); (g) sea-snake mimicry; (h) sea-snake model, banded sea-snake (Laticauda sp.). Photographs by permission M. Norman et al. 2001 [352].

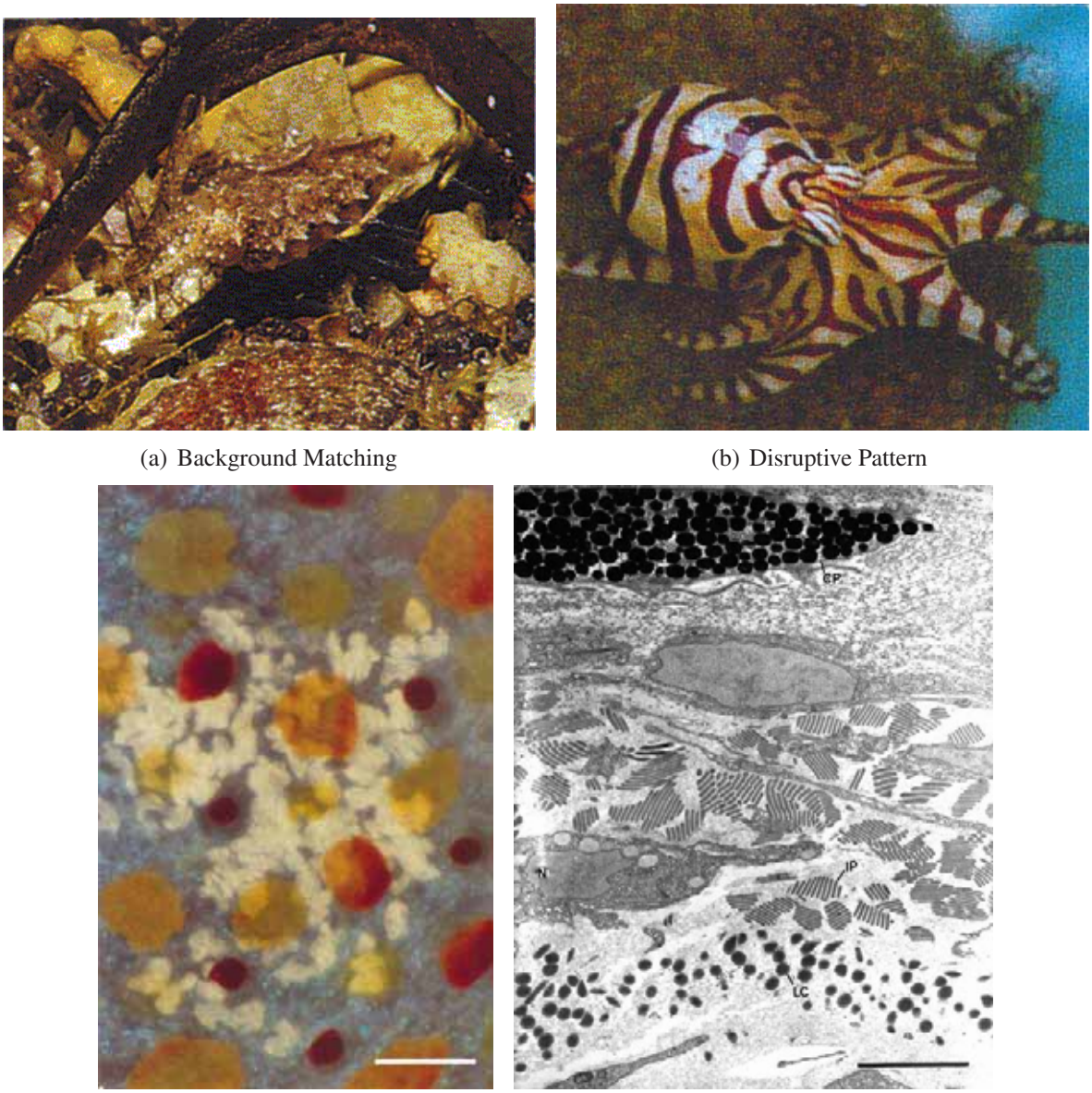

(a) Background Matching

(b) Disruptive Pattern

(c) Skin Patch

(d) Cross Section

Figure 5.8: Examples of cephalopod camouflage. (a) *S. officinalis* hatchling conceals itself with major lateral papillae and raised arms (mantle length 10 mm). Messenger 2001 [325]. (b) *Octopus zonatus* shows disruptive pattern (mantle length, 30 mm). Hanlon 1988 and Messenger 2001 [195]. (c) *Octopus vulgaris* chromatophore unit. Underlying leucophores reflect white and iridophores appear as small blue-green. Scale bar 50 μm. Froesch and Messenger, 1978 [167]. (d) Low-power electron micrograph of a vertical skin section of *Octopus vulgaris* shows a chromatophore (CP) above iridophores (IP) and leucophores. IP for iridosomal platelets, N for nucleus, and LC for leucophore clubs. Scale bar 5 μm. Froesch and Messenger, 1978 [167].

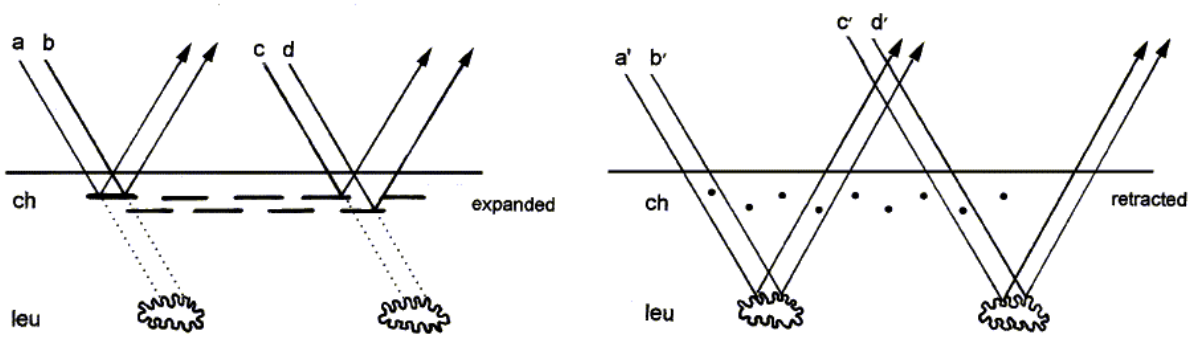

(a) Bright Background (b) Low-light Background

Figure 5.9: Schematics of background matching with chromatophores (ch) and leucophores (leu). (a) The chromatophores contract their muscle fibers and expand to absorb light and let their pigment color show for well-lit backgrounds. (b) The chromatophores relax and reduce their size for low-light backgrounds. This uncovers the leucophores that reflect the background light. Messenger 2001 [325].

The octopuses match the colors in a well-lit background by selectively contracting the chromatophore muscles that control the relative sizes of the differently colored chromatophores. *Octopus vulgaris* has yellow, orange, red, brown, and black chromatophores [360]. The iridophores refract light to give green, cyan, and blue colors. The uncovered leucophores reflect background light so can match the background color.

A single chromatophore receives multiple innervation so it can participate in different patterns [325]. The skin papilla muscles contract and turn a skin patch into a spike. This can match the smooth or rough texture of a background [360].

The chromatophores in an octopus and other cephalopods are neuromuscular organs [325]. A cephalopod uses neural control of the chromatophore organs to change its appearance almost instantaneously [325]. Each chromatophore consists of a pigment-containing elastic sacculus that attaches to a set of obliquely striated radial muscles. Each radial muscle has its own nerves and glia. The excited muscles contract to expand the chromatophore. The relaxed muscles allow the elastic sacculus to retract the chromatophore (see Figure 5.10).

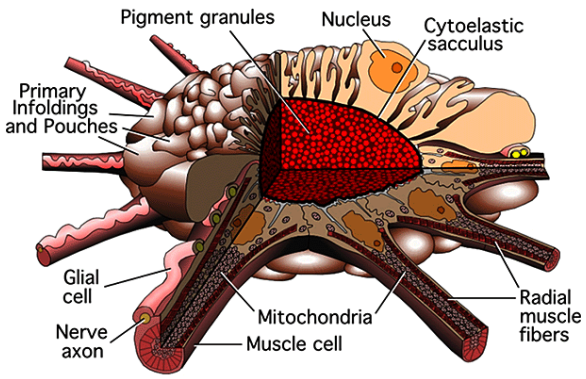

Figure 5.10: Cephalopod chromatophore organ. The figure is a retracted chromatophore from the squid, *Loligo opalescens*. Messenger 2001 [325].

Figure 5.11: The cephalopod next to a white stone displays a white square. A plastic ruff placed around the "neck" of *Sepia officinalis* (mantle length 120 mm) prevents it from seeing its own mantle but does not prevent it from showing an appropriate disruptive pattern, which includes such distinctive components as the White square. Messenger 2001 [325].

Octopus vulgaris has more than a million neurons in the chromatophore lobes. Specific nerve fibers innervate groups of chromatophores within fixed morphological arrays and so produce visible chromatomotor fields [325]. Researchers believe that the skin patterns are hard-wired. But the mimic octopuses [352] suggest that at least a part of the camouflage behavior is learned. Figure 5.11 shows a cephalopod that adapts its gross disruptive patterns to mimic a nearby object.

5.3.2 A Proposed Adaptive Camouflage Models *Octopus vulgaris*

A proposed adaptive camouflage can help conceal armor by modeling octopuses to match camouflage patterns to backgrounds. The proposed architecture loosely follows the schematic in Figure 5.9. Artificial color organs can display programmable patterns. And nanotube detectors and processors can select a camouflage pattern that optimally matches a background.

A prototype adaptive camouflage may use available components. Researchers have developed a color-change gel in Figure 5.12(a) that models octopus chromatophore organs. Commercial cadmium selenide (CdSe) semiconductor quantum dots or q-dots in Figure 5.12(c) can be superior pigments in artificial chromatophores. Retro-reflective materials in Figure 5.12(d) can be efficient artificial leucophores. Nanotube-based actuators [192] can implement artificial papillae that alter surface textures.

Programmable MR-treated fabrics can help an armor user maintain a posture to remain hidden. The MR-treated armor can programmably stiffen [231] [116] to support joints and so can help with posture.

Nanotube signal processing should further help disguise armor by approximating invisibility. Researchers have demonstrated an "optical camouflage" [433] that approximates invisibility by duplicating the background image. The adaptive camouflage should approximate invisibility by simulating a transmissive medium at the pixel level.

Nanotubes and nanoparticles can model an artificial chromatophore organ or chromatomotor that consists of photoemitters, reflecter/scatterers, and photoabsorbers. Stimuli-responsive polymer particles [8] can combine with mature products such as CdSe q-dots [385] and retro-reflective beads and prisms [393] to produce prototype chromatomotors. A 20–60 μm diameter particle of N-isopropylacrylamide (NIPAM) polymer shrinks by a factor of ten for heating that increases the temperature to 34 °C

from room temperature [8]. Particles smaller than 20 μm in diameter absorb light poorly so the shrunken particles show little color [8].

Commercial CdSe q-dots should improve the pigments in [8] because q-dots are more stable than most dye and offer many more color choices. A 50 μm diameter bead rests on a reflective surface and reflects an incident light back to its source [433] with high reflective efficiency.

Commercial retro-reflective beads should improve the leucophores [393]. *Octopus vulgaris* chromatophores measure 300 μm in diameter (see Figure 5.9(a)) so an artificial chromatophore of a similar size would use tens of NIPAM particles and reflective beads.

One possible architecture resembles a modified liquid-crystal display (LCD) (see Figure 5.9(b)): The expanded polymer particles display color from the q-dots and cover the retro-reflective beads in each artificial chromatomotor pixel. Other possible architectures can use electromechanical switches to cover and uncover the q-dots and the reflectors or use switchable reflective substrates [295].

The artificial chromatophores can incorporate a light source to conceal an armor user in backlit conditions or when the armor user appears darker than the background (see Figure 5.13). An ultraviolet emitter can stimulate a cluster of artificial chromatophores and cause their q-dots to emit light [385] in low-light conditions. Nanotube field emitters can generate ultraviolet light [349] with an electron beam.

Effective camouflage requires only a fixed set of patterns that can match most backgrounds as the octopuses demonstrate. A central control architecture models the optic-lobe controlled camouflage in an octopus that selects an optimal pattern based on visual information.

A camouflage pattern can be hardwired for designed patterns (Figure 5.14) and can also be adapted for new or changing patterns. An adaptive camouflage can take

(a) Expanded Color-change Gel

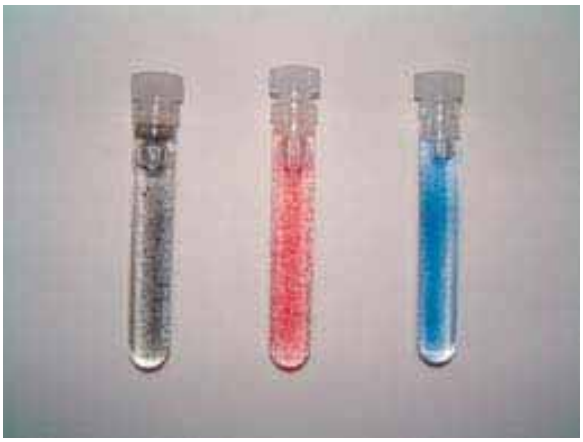

(b) Shrunken Color-change Gel

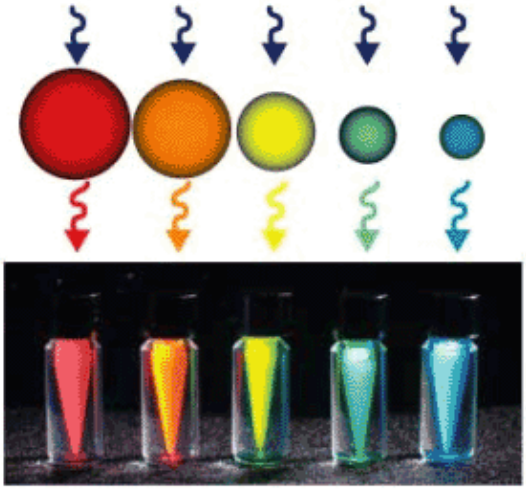

(c) CdSe Quantum Dots

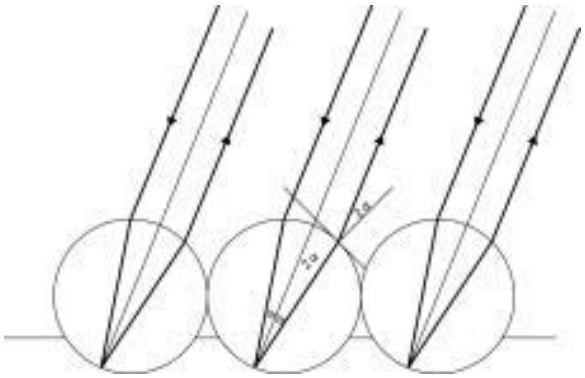

(d) Micron-scale Beads

Figure 5.12: Micro and nano scale materials for adaptive camouflage. (a) and (b) Dispersions of color change gel particles that contain black, magenta and blue dye. (a) Expanded state at 20 °C. (b) Shrunken state at 40 °C. With permission from R. Akashi [8]. (c) Vials of nano scale quantum dots under UV illumination. The colored spheres illustrate the relative sizes of the CdSe quantum dots in the vials. Quantum Dot Corporation, online http://www.qdots.com (d) Micron scale beads converts a reflective surface into a retro-reflective surface: Light reflects back toward the source. With permission from S. Tachi [433].

a snapshot of its surroundings, compare the image sample with stored patterns, and select the best hardwired pattern using little computation.

Figure 5.13: Matching background brightness and color improves camouflage. The center soldier appears brighter than the surroundings. The fourth soldier on the right appears darker than the immediate surroundings. This shows that brightness-matching and color-matching improves camouflage effectiveness. Photograph by permission G. Cramer [97].

Nanotube photodetectors can be compact and sensitive and fit in ultra-dense arrays (see Chapter 2 for more discussions). An all-nanotube architecture for signal processing and interconnection can operate at high speeds. This nanotube signal processing can process the visual information, assemble a combination of fixed patterns, and control an array of photoemitters such as the artificial chromatomotors.

Pure singlewall nanotube fibers [150] have strength and conductivity that suggest super-strong and conductive fabrics that can be part of the armor and can connect the detector array to the signal processing integrated circuits. The nanotube sensors and circuits can also integrate on a flexible conductive polymer substrate [479] that covers the armor.

Adaptive camouflage can approximate invisibility if it precisely duplicates the background. A so-called "optical camouflage" duplicates the background perfectly

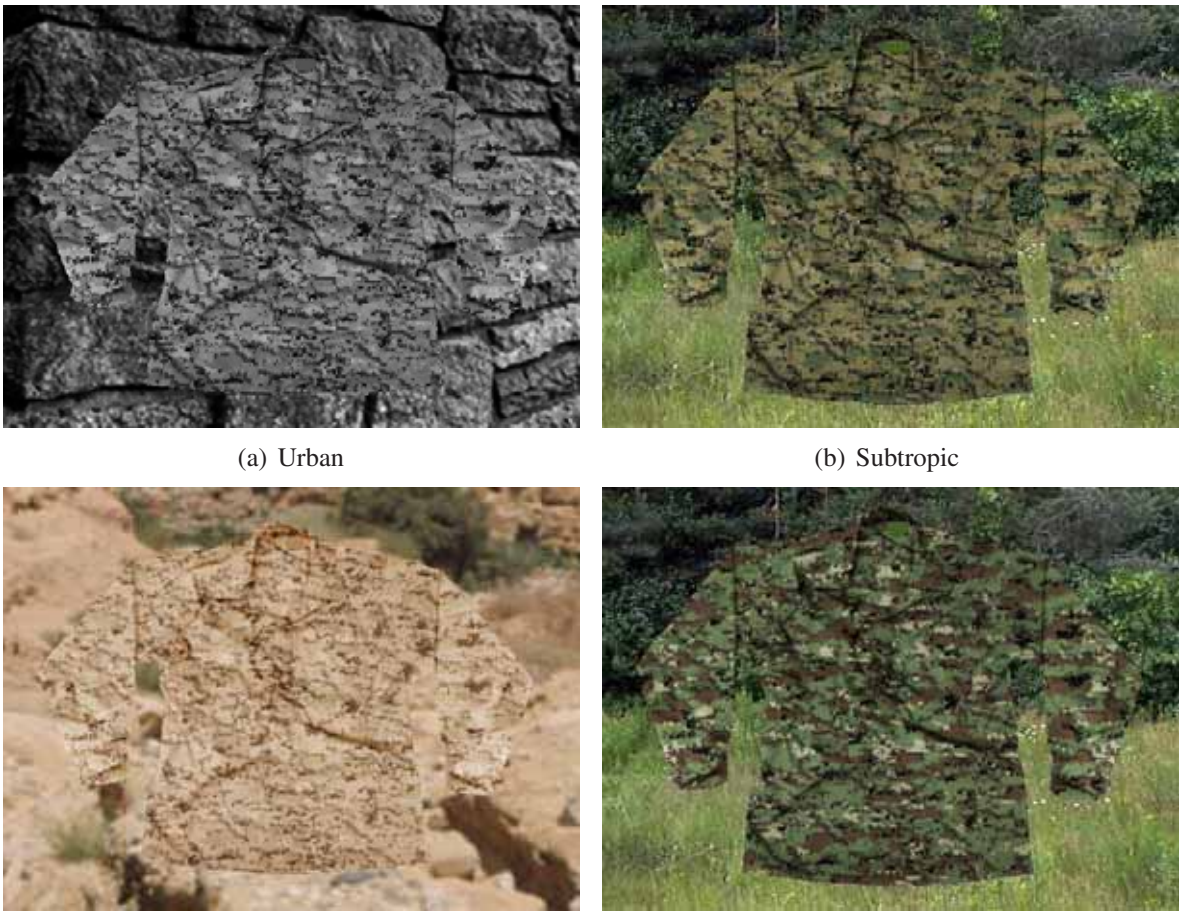

(a) Urban (b) Subtropic

(c) Desert (d) Woodland

Figure 5.14: Designed camouflage patterns. The designer developed these camouflage patterns using proprietary graphics techniques known as Camouflage Designated Enhanced Fractal Geometry. Photographs courtesy of G. Cramer [96].

but only from certain viewing positions (see Figure 5.15). True invisibility requires duplicating almost all incident light as if the light passed through air.

Nanotube signal processing may approach invisibility at the pixel level: A high-resolution wide-area array of photodetectors samples the incident light. A similarly distributed array of photoemitters displays the sampled image. A central or distributed signal processor extracts the frequency, phase, amplitude, and angle of arrival from the

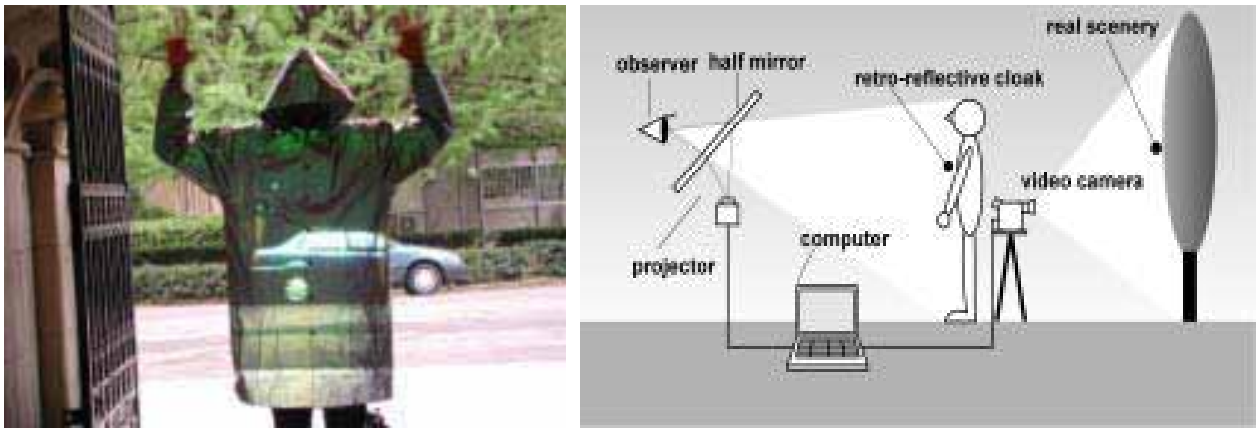

(a) Optical Camouflage (b) Video Projection

Figure 5.15: Video projection produces near invisibility. A camera behind the person records the background for projection onto the person's cloak. The cloak has a coating of retro-reflective material. S. Tachi 2003 [433].

sampled image and computes the weights for each emitter to duplicate the optical field for almost all viewing positions. This should resemble a holographic display.

Nanotube high-speed computation [67] may perform the image and array signal processing in real time with a reduced resolution. Nanotube interconnection, switches, sensors, and emitters can enable compact and low-power designs.

Single-electron transistor-based artificial molecules can improve on the octopus model. True hologram-like invisibility may be possible with large arrays of nanoscale photodetectors, emitters, and distributed signal processors. One such nanoscale emitter may be a CNT-SET-based artificial molecule that can tune its emission frequency.

The artificial molecules can emit light using the same principle as the semiconductor quantum dots [385]: Excited electrons emit photons with energy equal to or greater than the semiconductor bandgap to return to its ground state. Each semiconductor nanoscale dot has an electronic density of states with a size-dependent bandgap. So a SET-based artificial molecule can tune its emission frequency because it can alter the electronic density of states by adding single electrons [319].